Fluid modelling of a packed bed dielectric barrier discharge plasma reactor

Reference:
Van Laer Koen, Bogaerts Annemie.- Fluid modelling of a packed bed dielectric barrier discharge plasma reactor
Plasma sources science and technology / Institute of Physics - ISSN 0963-0252 - 25:1(2016), 015002
Full text (Publishers DOI): http://dx.doi.org/doi:10.1088/0963-0252/25/1/015002

Fluid modelling of a packed bed dielectric barrier discharge plasma reactor

Koen Van Laer[1], Annemie Bogaerts[1]

[1] Research group PLASMANT, Department of Chemistry, University of Antwerp, Universiteitsplein 1, 2610 Wilrijk-Antwerp, Belgium

E-mail: koen.vanlaer@uantwerpen.be

Abstract

A packed bed dielectric barrier discharge plasma reactor is computationally studied with a fluid model. Two different complementary axisymmetric 2D geometries are used to mimic the intrinsic 3D problem. It is found that a packing enhances the electric field strength and electron temperature at the contact points of the dielectric material due to polarization of the beads by the applied potential. As a result, these contact points prove to be of direct importance to initiate the plasma. At low applied potential, the discharge stays at the contact points, and shows the properties of a Townsend discharge. When a high enough potential is applied, the plasma will be able to travel through the gaps in between the beads from wall to wall, forming a glow-like discharge. Therefore, the inclusion of a so-called “channel of voids” is indispensable in any type of packed bed modelling.

1. Introduction

Dielectric barrier discharges (DBDs) have been of interest for quite some time, for various applications at atmospheric pressure [1]. For environmental applications, such as gaseous pollutant removal or the conversion of greenhouse gases into value-added chemicals, this type of plasma can be an interesting alternative for conventional thermal methods, because the input energy solely goes to heating up the electrons, while the gas itself may stay at room temperature. However, the energy efficiency that can be obtained, e.g., for CO_2 conversion, is rather limited [2-4]. In order to overcome this limitation, a dielectric packing has been introduced in the gas gap of the reactor, forming a so-called packed bed plasma reactor (PBPR). Some commonly used dielectrics are glass (dielectric constant ~4-6), quartz (dielectric constant ~4-7), aluminium oxide (dielectric constant ~10), zirconium oxide (dielectric constant ~10s), titanium oxide (dielectric constant ~100s), ceramic (dielectric constant ~10s-10000s) and ferroelectric materials (dielectric constant ~100s-10000s) [5].

This type of reactor has been widely experimentally investigated in the last few years in applications like ozone generation [6-8], gaseous pollutant removal [9, 10], H_2 production [11, 12] and CO_2 conversion [13-15], resulting in a significant improvement in energy efficiency, up to a factor 12 [8]. The improvement is suggested to be attributed to the increased electric field at the various contact points of the packing beads with each other and with the walls, due to the polarization of these materials. This strong electric field induces a locally higher electron temperature and thus higher reaction rates, but also a lower plasma density [16]. In comparison with an empty DBD reactor, the amount of surface area where a low permittivity (the gas) is in contact with a high permittivity (alumina, zirconia dielectrics), is also increased. At these boundaries, electric field enhancement will take place, enhancing the formation of ionization waves. However, the underlying mechanisms of plasma formation and behaviour are still poorly understood in a PBPR. In order to improve the applications, a better understanding of the packing effect is crucial. Plasma diagnostics, e.g., by probes, optical emission or laser diagnostics, are not straightforward in a PBPR, as the optical and physical access is limited due to the presence of the beads. Therefore, a computational approach is very much of interest to gain more insight.

In the past, only a few numerical studies have been performed for packed bed DBD reactors [17-20]. Chang and Takaki et al. [17, 18] developed a simplified 1D parallel plate N_2 plasma model, focusing on the determination of the electron density, electron energy and electric field strength, based on the applied voltage, the distance between the electrodes, the free volume and the dielectric constants of the beads and the gas. Because of the 1D model, the void between the beads was assumed to be spherical. Kang et al. [19] developed a 2D model to study the impact of introducing dielectric beads in a parallel plate DBD reactor on the evolution and characteristics of the typical microdischarges. The model studied two packing beads directly on top of each other, without the inclusion of plasma chemical reactions. Finally, Russ et al. [20] used a 2D hydrodynamic model, to study transient microdischarges in a packed bed DBD reactor filled with dry exhaust gas (80% N_2, 20% O_2 and 500 ppm NO). This model included an extensive chemical reaction set with 23 different species reacting in 120 different plasma reactions, simulating a short one-directional discharge (of a few 10s of nanoseconds) via a constant applied potential difference. A void channel through the packing from one wall to the other (see below) was, however, not present in their geometry.

In principle, a PBPR should be studied in three dimensions to take into account the packing geometry as it is in real life. However, the duration of such 3D simulations is estimated to be

well over a few months on today's modern computers, for just a couple of periods of the applied potential, at the conditions under study in our work (geometry, applied potential, frequency, gas mixture and pressure). Due to these computational limitations, a 2D model is needed to gain the first insights in the mechanism of a plasma discharge in a PBPR. It is of course key in such model to simplify the 3D geometry without compromising its authenticity. With this study, we hope to obtain more insight into the formation and behaviour of a plasma in a PBPR at atmospheric pressure, as well as on the influence of the applied potential on the discharge formation.

2. Model description

Using COMSOL's built-in plasma module, a two-dimensional axisymmetric fluid model is developed with semi kinetic treatment of the electrons (see below). The model is based on solving a set of coupled differential equations that express the conservation of mass, momentum and energy, for the different plasma species. The mass conservation equation is as follows:

$$\frac{\partial n_i}{\partial t} + \nabla \cdot \mathbf{\Gamma_{i,j}} = S_i$$

n_i stands for the density of the plasma species i, which can be an electron, ion, radical or neutral species. $\mathbf{\Gamma_{i,j}}$ is its flux, and S_i is the source term, which is the sum of the production and loss terms for this species, based on the chemical reaction set (see below):

$$S_i = \sum_r c_{i,r} R_{i,r}$$

$c_{i,r}$ is the stoichiometric coefficient of species i in reaction r, and $R_{i,r}$ the reaction rate. The conservation equation of momentum is not explicitly solved, but is replaced by an expression for the flux, based on the drift-diffusion approximation:

$$\mathbf{\Gamma_{i,j}} = \mu_{i,j} n_i \mathbf{E} - D_{i,j} \nabla n_i$$

The first term describes the electric drift, with $\mu_{i,j}$ the mobility and **E** the electric field, and will only be solved for the electrons and the ions. The second term stands for the diffusion, with D_i the diffusion coefficient. This term is solved for all species. The third conservation equation describes the electron energy:

$$\frac{\partial n_\varepsilon}{\partial t} + \nabla \cdot \mathbf{\Gamma_{\varepsilon,j}} = S_\varepsilon$$

n_ε is the electron energy density (i.e., the product of electron density n_e and mean electron energy $\bar{\varepsilon}$), S_ε is the source term for the electron energy and $\mathbf{\Gamma_{\varepsilon,i}}$ is the electron energy flux:

$$S_\varepsilon = -e\mathbf{\Gamma_{e,j}} \cdot \mathbf{E} + \sum_r c_r \bar{\varepsilon}_r R_r$$

$$\boldsymbol{\Gamma_{\varepsilon,j}} = \frac{5}{3}\mu_{e,j}\mathbf{E}n_\varepsilon - \frac{5}{3}D_{e,j}\nabla n_\varepsilon$$

The first term in the source term equation describes the Joule heating of the electrons by the electric field. The second term represents the change in electron energy due to chemical reactions, where $\bar{\varepsilon}_r$ is the energy lost or gained by one electron in reaction r. In the electron energy flux equation, $\mu_{e,j}$ and $D_{e,j}$ stand for the electron mobility and diffusion coefficient, respectively. From the electron energy and electron density, the electron temperature T_e can be calculated:

$$k_B T_e = \frac{2}{3}\bar{\varepsilon} = \frac{2}{3}\frac{n_\varepsilon}{n_e}$$

Finally, the Poisson equation will also be solved to self-consistently calculate the electric field distribution, using the densities of the different charged plasma species as input in the gas gap, and solving for zero space charge in the dielectric material:

$$\nabla \cdot (\varepsilon_0 \varepsilon_r \mathbf{E}) = -\nabla \cdot (\varepsilon_0 \varepsilon_r \nabla V) = \rho$$

ε_0 is the permittivity of vacuum, ε_r the relative permittivity of the material or the gas, V is the potential and ρ is the space charge density.

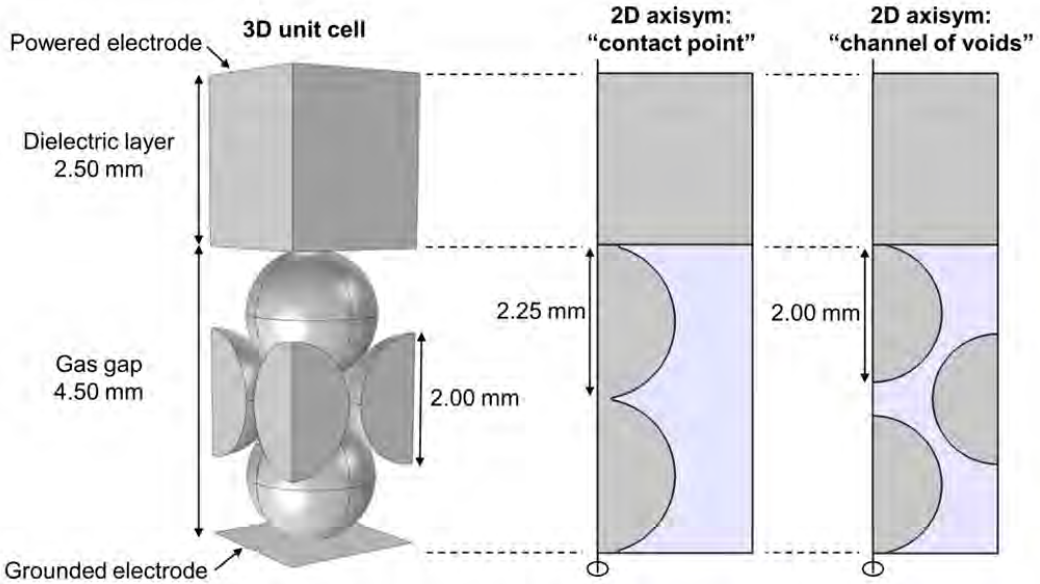

Fig. 1. 3D unit cell of the packed bed plasma reactor (PBPR) and its 2D representations used in the model.

Two different 2D axisymmetric geometries, based on a 3D unit cell of a close-packed PBPR are used to best represent the 3D problem (Fig. 1). The 3D unit cell contains two important geometrical properties, which need to be taken into account in the 2D adaptation. The contact

points between the dielectric materials (i.e. beads, walls) are the first property. The contact points will strongly change the electric field distribution in the gas gap and will therefore have a big influence on plasma generation and distribution throughout the gap. In addition, these contact points also cause the voltage-driven electrode to be in direct contact with the grounded electrode, through a "channel of dielectric material", lowering the electric field strength over the entire gap. We studied this phenomenon with simple electrostatic models (i.e. not including any plasma reactions) in 2D and 3D, but the results indicated that its influence was only minor. The second property is the existence of a so-called "channel of voids". Indeed, just like the fact that all the dielectric materials are linked, all the voids in between the beads are also connected to each other, resulting in a direct channel from the dielectric layer on top of the voltage-driven electrode to the grounded electrode. This channel must be present because the plasma must be able to travel from one side of the discharge gap to the other. However, it is not possible to make a single axisymmetric 2D adaptation of the 3D unit cell with both the "channel of voids" present and all the packing beads in direct contact. Therefore, two different geometries are studied, each focussing on one of the properties. In both geometries, the rotational axis is located on the left side.

The first geometry shows two packing beads made of zirconia (dielectric constant, $\varepsilon_r = 25$) with diameters of 2.25 mm, on top of each other, making direct contact with each other and with the walls, which are 4.5 mm apart. We selected zirconia as the packing material, because of our earlier experimental work with this material [15]. In our future work, we plan to investigate the effect of different materials with different dielectric constants on the plasma behaviour in the PBPR. A 2.5 mm thick layer of alumina ($\varepsilon_r = 9$) is covering the voltage driven electrode. To overcome computational difficulties due to extreme mesh requirements, the contact points are slightly enlarged and rounded. This geometry will be called the "contact point model".

The second geometry shows three packing beads, i.e., two beads on the left, with (the real) diameter of 2.00 mm and spaced apart so that they both are in contact with the opposite wall, leaving a gap of 0.5 mm in between. On the right side, another packing bead was added to create the "channel of voids"; therefore we will call this the "channel of voids model". It must be realized that this packing bead after rotation around the axis will not be a sphere but a torus. Thus, both geometries are not a true copy of the real life geometry, but they can give us insights into the real life plasma behaviour.

As stated before, these models require a very fine mesh, due to the presence of the round edges of the packing beads and the sharp corners at the contact points. Triangular meshing is used across the whole geometry, except at the walls, where rectangular meshed boundary layers are added to better resolve the sheath formation. The distance between two mesh points in the gas gap is limited to 10 μm, and it is an order of magnitude smaller at the contact points. At the material surfaces, the distance between two mesh points is also limited to 1μm, in order to reach a good enough smoothness. Inside the dielectric material, the mesh is allowed to be coarser. As a result, the "contact point model" and the "channel of voids model" consist of 91202 and 73300 mesh elements, respectively. We performed a sensitivity study of the required mesh resolution, and found that a computation with less mesh points can lead to spike formation, whereas a calculation with more mesh points yields the same results but will only take longer.

Nr.	Reaction	Rate coefficient	Reference
R1	$e + He \rightarrow He + e$	cross-section	21
R2	$e + He \rightarrow He^* + e$	cross-section	21

R3	$e + He^* \rightarrow He + e$	cross-section	22
R4	$e + He \rightarrow He^+ + 2e$	cross-section	21
R5	$e + He^* \rightarrow He^+ + 2e$	cross-section	21
R6	$e + He_2^* \rightarrow 2He + e$	3.8×10^{-15} cm^3 s^{-1}	23, 24
R7	$2e + He^+ \rightarrow He^* + e$	$6.0 \times 10^{-20} (T_e/T_g)^{-4.4}$ cm^6 s^{-1}	24
R8	$2e + He_2^+ \rightarrow He^* + He + e$	$4.0 \times 10^{-20} (T_e/T_g)^{-1}$ cm^6 s^{-1}	24
R9	$e + He_2^+ + He \rightarrow He^* + 2He$	$5.0 \times 10^{-27} (T_e/T_g)^{-1}$ cm^6 s^{-1}	24
R10	$2e + He_2^+ \rightarrow He_2^* + e$	$4.0 \times 10^{-20} (T_e/T_g)^{-1}$ cm^6 s^{-1}	24
R11	$e + He_2^+ + He \rightarrow He_2^* + He$	$5.0 \times 10^{-27} (T_e/T_g)^{-1}$ cm^6 s^{-1}	24
R12	$e + He_2^* \rightarrow He_2^+ + 2e$	$9.75 \times 10^{-10} T_e^{0.71} e^{-3.4/Te}$ cm^3 s^{-1}	24
R13	$e + He^+ + He \rightarrow He^* + He$	$1.0 \times 10^{-26} (T_e/T_g)^{-2}$ cm^6 s^{-1}	24
R14	$e + He_2^+ \rightarrow He_2^*$	$5.0 \times 10^{-9} (T_e/T_g)^{-1}$ cm^3 s^{-1}	24
R15	$He^* + He^* \rightarrow He_2^+ + e$	$2.03 \times 10^{-9} (T_g/0.025)^{0.5}$ cm^3 s^{-1}	24
R16	$He^* + He^* \rightarrow He^+ + He + e$	$8.7 \times 10^{-10} (T_g/0.025)^{0.5}$ cm^3 s^{-1}	24
R17	$He^+ + 2He \rightarrow He_2^+ + He$	$1.4 \times 10^{-31} (T_g/0.025)^{-0.6}$ cm^6 s^{-1}	24
R18	$He^* + 2He \rightarrow He_2^* + He$	$8.1 \times 10^{-36} T_g$' $e^{-650/Tg'}$ cm^6 s^{-1}	24
R19	$He_2^* + He^* \rightarrow He^+ + 2He + e$	$2.03 \times 10^{-9} (T_g/0.025)^{0.5}$ cm^3 s^{-1}	24
R20	$He_2^* + He^* \rightarrow He_2^+ + He + e$	$8.7 \times 10^{-10} (T_g/0.025)^{0.5}$ cm^3 s^{-1}	24
R21	$He_2^* + He_2^* \rightarrow He^+ + 3He + e$	$2.03 \times 10^{-9} (T_g/0.025)^{0.5}$ cm^3 s^{-1}	24
R22	$He_2^* + He_2^* \rightarrow He_2^+ + 2He + e$	$8.7 \times 10^{-10} (T_g/0.025)^{0.5}$ cm^3 s^{-1}	24
R23	$He_2^* + He \rightarrow 3He$	4.9×10^{-22} cm^3 s^{-1}	23

Table: Helium reaction set with rate coefficients, and references where these data are adopted from. T_e is the electron temperature (eV), T_g the gas temperature in eV and T_g' the gas temperature in K.

Although this PBPR is mainly used for environmental applications, and thus in molecular gases, we apply the model in first instance to helium as the discharge gas, for two reasons. First of all, the reaction chemistry of this noble gas is quite simple, therefore limiting the calculation time. Second, it has the ability of forming a homogeneous instead of a filamentary discharge in a DBD reactor, and this is what we will be simulating by using a fluid model to describe the plasma. We focus here on the influence of a packing on the plasma formation and behaviour in a DBD reactor that would otherwise (without the packing) form a homogeneous discharge (i.e., using He as discharge gas). Since this is normally not the case for molecular gases, this limits the applicability of the obtained results. However, the insights that are gained from this study will certainly be helpful for future research on PBPR with more complex molecular gases.

The model considers six different species, i.e., electrons (e), neutral helium atoms (He), positive helium atomic and molecular ions (He^+, He_2^+), metastable helium atoms, He(2^1S) and He(2^3S) combined into one effective level He*, and helium dimers (He_2*). The different species interact with each other by 23 elementary reactions (Table 1). The rates of the first five reactions (R1-R5) are obtained by Bolsig+, a software program that solves the Boltzmann equation for the electrons, using the input collision cross-sections from the LXcat database, to generate the electron impact reaction rates as a function of the mean electron energy [21, 22]. It also calculates the transport coefficients of the electrons as a function of mean energy. The reaction rate coefficients of the other 18 reactions (R6-R23), namely recombination reactions with electrons and heavy particle reactions between ions, atoms and excited species, are taken from literature, and are typically a function of electron temperature or gas temperature [23, 24].

However, we assumed a constant gas temperature of 300 K. Indeed, our experiments revealed that the gas itself does not heat up in a PBPR with a gas flow as low as 20 mL min^{-1}. In the present model, we do not apply a gas flow. Since the model goes to steady state in only a few periods of applied potential, this is a correct representation of reality. However, since we do not have the inflow of "cool" gas, the gas might heat up if we would calculate it from the applied power, which would not reflect the reality of a gas flow. Therefore, we opted to keep the gas temperature constant. The mobilities $\mu_{i,j}$ of the ions are taken from literature [25], namely 1.0×10^{-3} m^2 V^{-1} s^{-1} for He^+ and 1.6×10^{-3} m^2 V^{-1} s^{-1} for He_2^+, and the corresponding diffusion coefficients $D_{i,j}$ are obtained from the Einstein relation.

$$D_{i,j} = \mu_{i,j} k_B T$$

This yields values of 2.6×10^{-3} m^2 s^{-1} and 4.1×10^{-3} m^2 s^{-1} for He^+ and He_2^+, respectively. For the neutral species, the diffusion coefficients are calculated with the Chapman-Enskog equation [26].

$$D_{i,j} = \frac{3k_B T \sqrt{\frac{4\pi k_B T}{2\mu_{ij}}}}{16 p \pi \sigma_{ij}^2 \Omega_D(\Psi)}$$

$$\text{with } \Omega_D = \frac{A}{\Psi^B} + \frac{C}{e^{D\Psi}} + \frac{E}{e^{F\Psi}} + \frac{G}{e^{H\Psi}};\ \Psi = \frac{k_B T}{\varepsilon_{ij}};\ \sigma_{ij} = \frac{\sigma_i + \sigma_j}{2};\ \varepsilon_{ij} = \sqrt{\varepsilon_i \varepsilon_j}$$

In these equations k_B is the Boltzmann constant (1.38×10^{-23} J K^{-1}), T the gas temperature (K), p the total pressure (Pa), μ_{ij} the reduced mass (kg), σ_{ij} the characteristic length (m), $\Omega_D(\Psi)$ the dimensionless diffusion collision integral, Ψ the dimensionless temperature and ε_{ij} the depth of the Lennard-Jones potential for the He-He interaction (J). The parameters A-H were taken from literature [27]. The diffusion coefficients are calculated to be 1.68×10^{-4} m^2 s^{-1} for both the atomic neutral species, i.e. He and He^*, and 1.45×10^{-4} m^2 s^{-1} for the molecular species He_2^*. An initial density of 10^{14} m^{-3} is assumed for both the electron and total ion density. This is quite high, and artificial. However, we have checked the effect of this assumption, and it was clear that these input values did not change the solution. They only help the model to start up easier, which saves calculation time in the beginning.

In the model, the packing beads are treated as solid objects with conservation of charge. On the surface, charge accumulation is possible by means of the following boundary conditions:

$$\boldsymbol{n} \cdot (\mathbf{D_1} - \mathbf{D_2}) = \rho_s$$

$$\frac{\partial \rho_s}{\partial t} = \boldsymbol{n} \cdot \mathbf{J_i} + \boldsymbol{n} \cdot \mathbf{J_e}$$

In these equations **n** stands for the normal vector, $\mathbf{D_1}$ and $\mathbf{D_2}$ are the displacement fields on both sides of the boundary, ρ_s is the surface charge (C m^{-2}), $\mathbf{n} \cdot \mathbf{J}_i$ and $\mathbf{n} \cdot \mathbf{J}_e$ are the normal components of the ion and electron current densities at the wall, respectively.

Finally, the different plasma species can also react at the walls. More specifically, the following surface reactions are taken into account: quenching of helium atomic and molecular metastables, and electron-ion recombination of He^+ and He_2^+ ions to ground state helium atoms, with a probability of 0.05 to send out a secondary electron with energy of 5 eV [28]. The boundary condition for the electric potential at an electrode is a predefined value, namely 0 V on the grounded electrode and V(t) on the powered electrode, where V(t) represents a radio frequency sine wave. The outer boundary on the right side of the geometries (Fig. 1) is treated with an insulation boundary condition, setting the normal fluxes of electrons and electron energy on this boundary to zero, and a zero charge boundary condition, defining the normal electric displacement equal to zero. The combination of these two boundary conditions implies periodicity, with a normal zero gradient of charged species across the boundary.

The time-dependent solver is an implicit differential-algebraic solver (IDA) and uses variable-step, variable-order backward differential formula (BDF) methods for its integration, with a maximum order of 2. At each step, the nonlinear system is linearized by a Newton iteration, into the $A \cdot x = b$ form. This linear system is then solved with PARDISO, which stands for parallel sparse direct solver [29]. It uses LU factorization on a matrix A to find the solution x. The time steps are chosen automatically by the BDF solver, based on the relative and absolute tolerances that control the solution error. For all variables we chose to set these errors at 0.001. On average, the time steps lie between 10^{-7} and 10^{-10} s. Further details on the use of COMSOL can be found elsewhere [30].

3. Results and discussion

3.1. Contact point model

First we present the results for the "contact point model" with an applied sinusoidal voltage of 4.0 kV peak-to-peak at a frequency of 23.5 kHz.

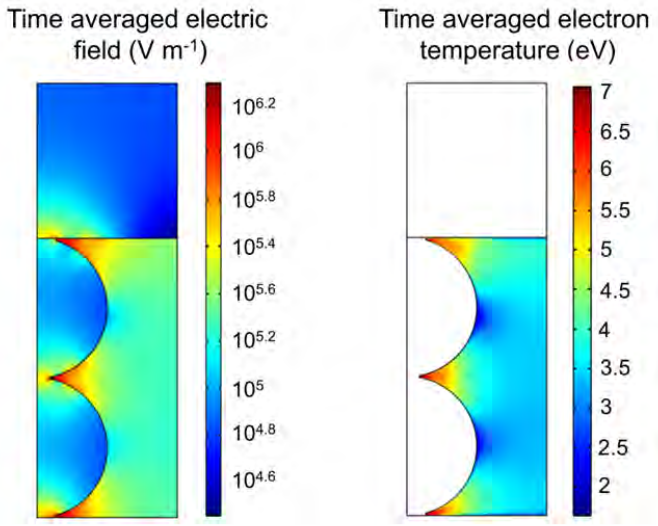

Fig. 2. Time averaged electric field strength (V m^{-1}) and electron temperature (eV) over one period of applied potential, i.e. 4.0 kV peak-to-peak at a frequency of 23.5 kHz.

Fig. 2 shows the time averaged electric field and electron temperature distributions over one period of applied potential. Due to the polarization of the packing beads as a result of the applied potential over these materials, the electric field at the contact points (both inside the materials and in the gas gap) will be enhanced. Hence, the electrons in this region will receive more energy than in the rest of the reactor. Therefore, when the breakdown voltage is reached, a discharge will be initiated at the contact points. When a low potential is applied, in our case 4.0 kV peak-to-peak, the discharge stays at this location, and behaves like a Townsend discharge: several low intensity current peaks per half cycle (equally spaced and decreasing in size; see Fig. 3 below), ion densities drastically exceeding the electron density, and an electric field that is weakly affected by the space charge [31-33]. The Townsend discharge is formed at two separate places in the reactor, namely at the contact point between the two dielectric beads, and at the contact point between the upper bead and the dielectric layer covering the powered electrode. At the contact point between the lower bead and the grounded electrode, no discharge will take place in spite of the considerable electric field, because of the presence of this electrode and thus, the lack of surface charge accumulation on its surface. Indeed, for a Townsend discharge the secondary electron yield from the surface is important to form a discharge [34]. The grounded metal electrode acts as a sink for charged species. If the grounded electrode would also be covered by dielectric material, a Townsend discharge would also be expected at the lower contact point.

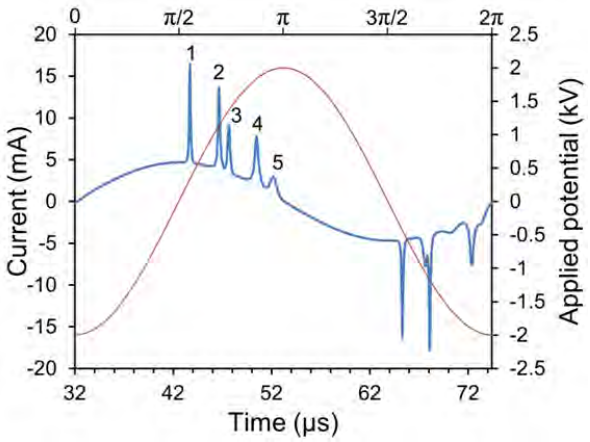

Fig. 3. Total current profile during one cycle of the applied potential of 4.0 kV peak-to-peak.

The total current profile, i.e., the sum of displacement and conduction current, during one half cycle of applied potential (Fig. 3) shows a superposition of two current profiles of Townsend discharges (i.e. consecutive equally spaced peaks, decreasing in size), one with three peaks, and one with two peaks. Peaks 1, 2 and 4 originate from three consecutive Townsend discharges at the contact point between the beads, while peaks 3 and 5 are from two Townsend discharges at the contact point of the upper bead with the dielectric layer. A similar pattern applies to the other half cycle, except for the fact that the superposition is slightly different. Indeed, the two discharges between the upper bead and the dielectric layer happen earlier in the cycle, before the second and third discharge at the contact point between the beads, respectively. The current waveform is reproducible from the second cycle onwards. The first (and sometimes also the second) cycle generally shows a little difference, attributed to the start-up of the model in the beginning. The initial conditions will not have an influence on the reproducible part of the current waveform. They can only fasten the start-up (as mentioned before).

The electron density distribution for the first breakdown at each of these places, in other words the electron density at the time of current peak 1 and 3, respectively, is shown in Fig. 4. These plots clearly show that the plasma is indeed formed locally, at different times during the half cycle. At 43.7 µs (left), a small plasma is formed at the contact point between the beads, while at 47.6 µs (right), the plasma is formed between the upper bead and the dielectric layer.

To further demonstrate the occurrence of Townsend discharges, the time averaged electron density and total ion density distributions are compared in Fig. 5. It is obvious that the ion density is up to two orders of magnitude higher than the electron density, as expected for a Townsend discharge. The electrons have a much higher mobility, due to their lower mass, so they move towards the walls, thereby charging the dielectrics. To verify, the surface charge density was calculated at any moment in time in the reactor and showed that it was negative at every time step, proving that the missing electrons from the bulk are indeed charging the surface. The amount of electrons on the surface was comparable to the amount missing from the bulk within the order of magnitude. The reason why they are not perfectly the same, lies in the fact that some stabilization is used in the model that artificially increases the amount of electrons in places where there are very few. The impact of this stabilization on the results was tested by comparing the model with a similar model without this stabilization present, and thus total charge conservation. This last model runs less stable, and therefore takes more time, but in the end it showed the same results as the model without stabilization. Figure 5 also shows that the plasma never leaves the region at the contact points, and has a rather low time averaged density. Finally, it is clear that indeed no discharge is formed at the contact point between the lower bead and the grounded electrode, as explained above.

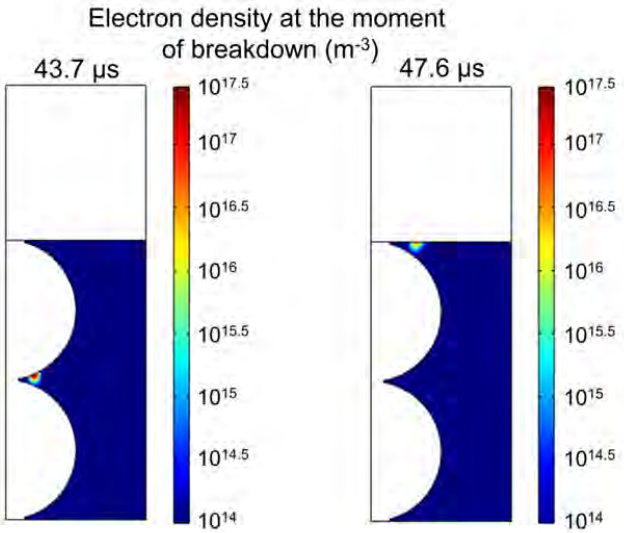

Fig. 4. Electron density (m^{-3}) at the moment of gas breakdown at the two separate contact points, i.e., corresponding to peak 1 (left) and peak 3 (right) of Fig. 3 above, for an applied potential of 4.0 kV peak-to-peak.

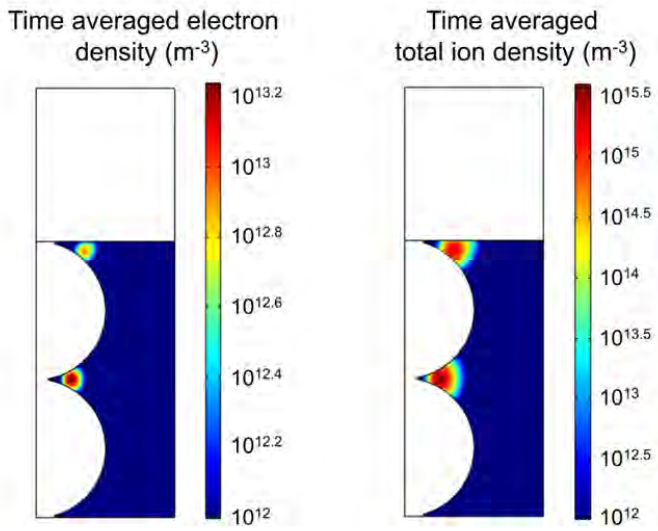

Fig. 5. Time averaged electron density (m^{-3}) and total ion density (m^{-3}) for an applied potential of 4.0 kV peak-to-peak.

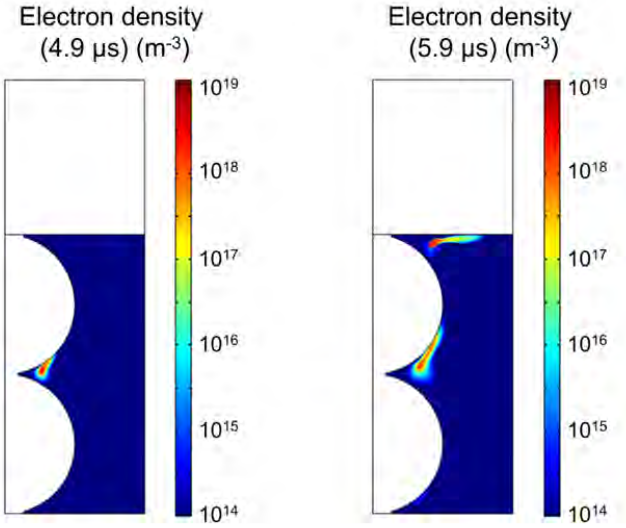

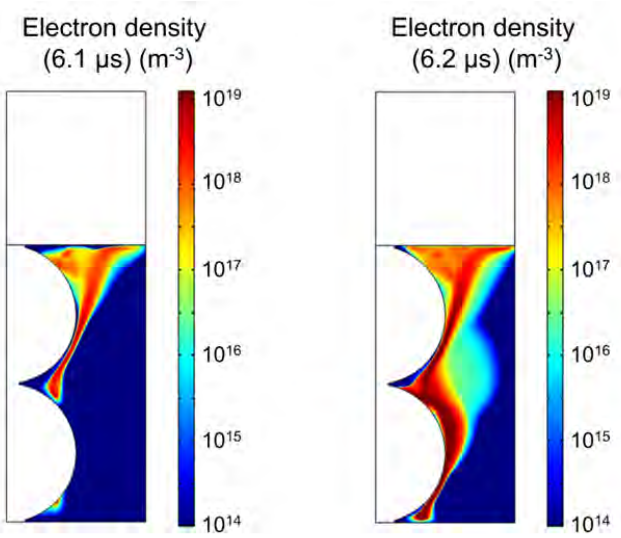

Fig.6. Instantaneous electron density (m^{-3}) at several consecutive moments in time after the moment of gas breakdown, indicating the course of events to form the final glow-like discharge, for an applied potential of 7.5 kV peak-to-peak.

When a higher potential, for instance 7.5 kV peak-to-peak, is applied, the discharge will still be initiated at the contact points. However, since the potential difference over the full gap distance is now much larger, the discharge will quickly spread out over the surface of the packing beads towards the bulk and form a glow-like discharge, which is proven by the presence of a quasineutral plasma. The discharge can best be seen as a homogeneous discharge as expected in an empty reactor, but deformed by the presence of the packing material. Just like in the paper of Golubovskii et al. for a non-packed DBD reactor [31], an ionization wave quickly travels towards the cathode when a discharge takes place (in a time frame of ns). This resembles the behaviour of a streamer. When it reaches the cathode, it creates a peak in the current, the spatial profile of the electric field changes and a glow-like discharge is formed that can last several µs. However, at the contact points, the discharge can quickly die out due to the small dimensions, which impede the formation of a quasineutral plasma zone. The course of events is illustrated in Fig. 6: the first discharge takes place at the contact point between the packing beads. Not much later, a second discharge is initiated at the contact point of the upper bead with the dielectric layer. Since the applied potential at this point is still increasing, a discharge can take place over the entire gap distance. However, because of the presence of the packing beads, and the accompanying electric field enhancement on the surfaces and at the contact points, the discharge will not be formed in the gap as expected for an empty reactor, but will be formed near the surface of the packing beads, from one contact point to the other. Fig. 7 shows the time averaged electron and ion density distribution from the moment at which the full discharge over the surface is formed (after 6.2 µs, Fig. 6 bottom right) until the end of the first half period, and illustrates the quasineutrality of the formed plasma discharge. The density of electrons tends to be a bit lower at the cathode surface (the dielectric layer) due to the presence of a cathode fall region. They also move faster through the bulk towards the nearby bead surfaces than the ions. Fig. 7 also indicates that we are not dealing with a streamer discharge remnant, which would show a much higher ion density than electron density [35], but an actual glow-like discharge that lasts for several µs.

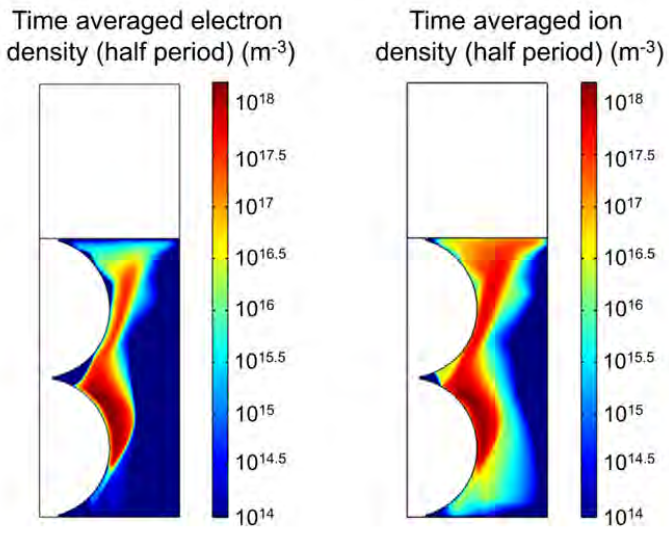

Fig.7. Time averaged electron density (m^{-3}) and total ion density (m^{-3}) from 6.2 μs until the end of the first half period, for an applied potential of 7.5 kV peak-to-peak.

3.2. Channel of voids model

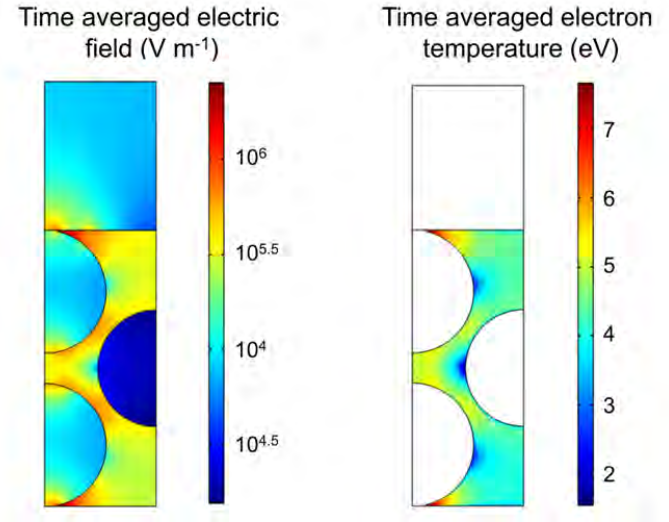

Fig. 8. Time averaged electric field strength (V m^{-1}) and electron temperature (eV) over one period of applied potential of 4.0 kV peak-to-peak with a frequency of 23.5 kHz.

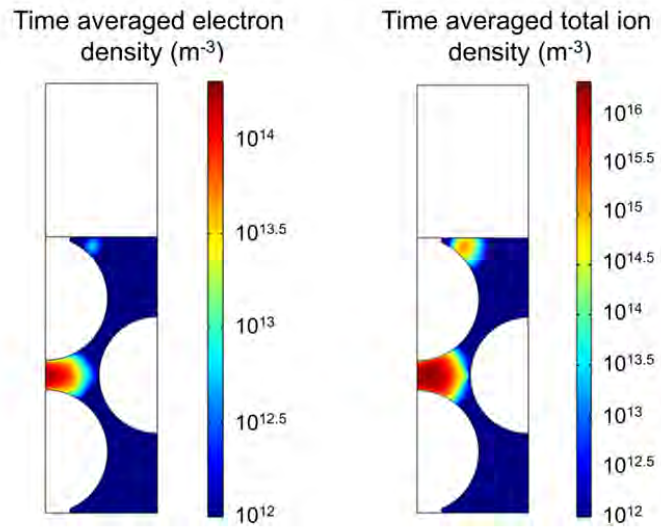

Fig. 9. Time averaged electron density (m^{-3}) and total ion density (m^{-3}) for an applied voltage of 4.0 kV peak-to-peak.

At low applied potential of 4.0 kV peak-to-peak, the "channel of voids model" shows similar results as the "contact point model". Again the electric field strength and electron temperature are strongly influenced by the presence of the packing beads and their polarisation, resulting in maxima near the contact points (Fig. 8). The values are slightly different because of the different geometry approximations, and the reality will probably be somewhere in between. Plasma initiation takes place between the two packing pellets on the left and at the contact point of the upper bead with the dielectric layer that covers the powered electrode, similar to the "contact point model". Again the discharges stay in these regions and are Townsend-like, as demonstrated by the time averaged electron and ion density distributions, showing the absence of a quasineutral plasma (Fig. 9). The current profile over one half cycle of applied potential is not shown because it is almost identical to the current profile of the "contact point model" (Fig. 3).

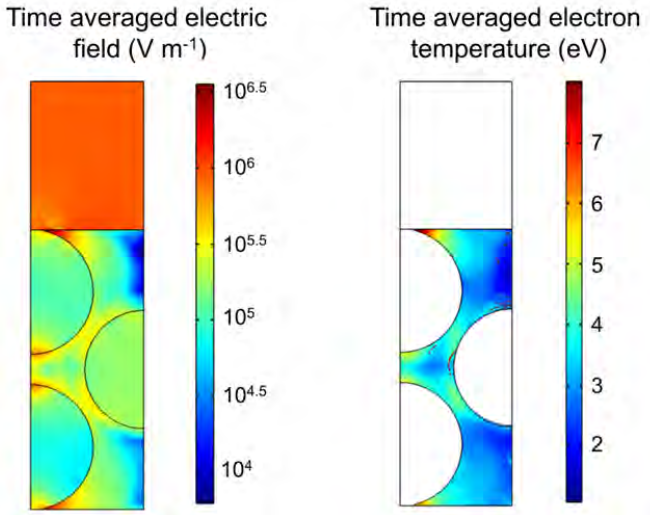

Fig. 10. Time averaged electric field strength (V m^{-1}) and electron temperature (eV) over one period of applied potential of 7.5 kV peak-to-peak with a frequency of 23.5 kHz.

When the applied potential is increased to 7.5 kV peak-to-peak, the discharge behaviour changes drastically, with the third packing bead coming more into play. The electron temperature and electric field strength are still at maximum at the contact points, but typically show a lower value above and below the right packing bead (Fig. 10). This lower value is caused by the presence of a quasineutral plasma in these regions during most of the half cycle of the applied potential. Due to its high density, the resulting space charge strongly affects the external electric field. The discharge is no longer Townsend-like, but behaves more glow-like.

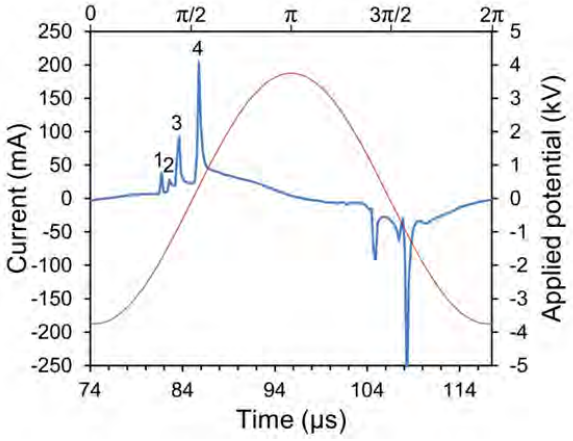

Fig. 11. Total current profile during one cycle of the applied potential of 7.5 kV peak-to-peak.

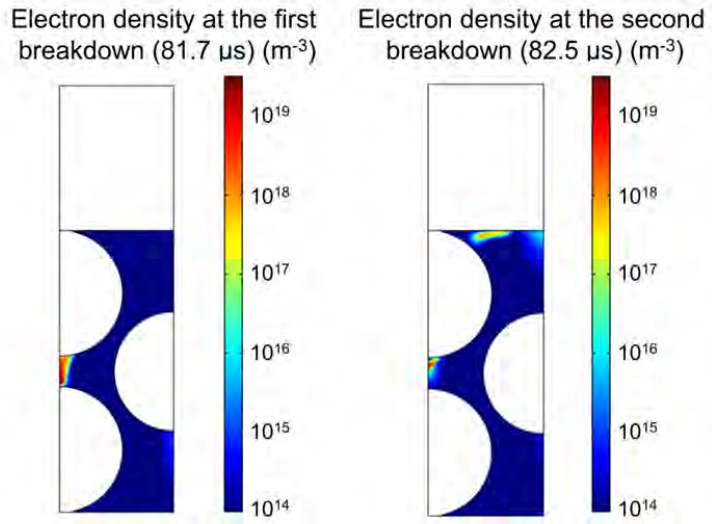

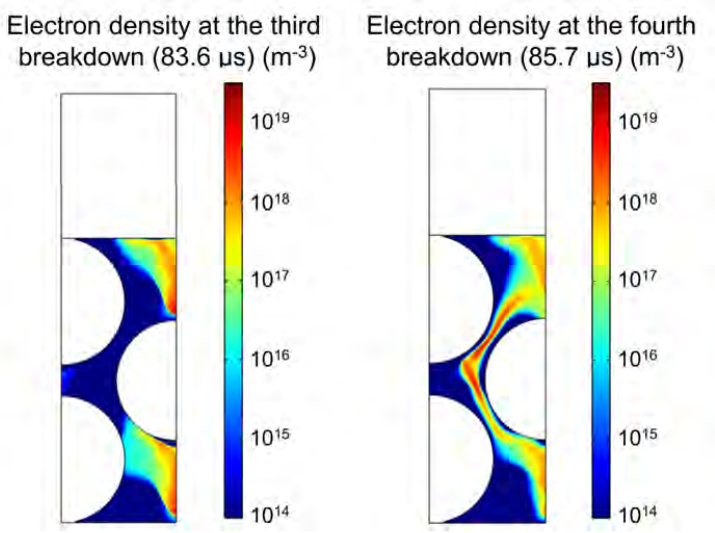

Fig. 12. Electron density (m^{-3}) at four consecutive moments of gas breakdown for an applied potential of 7.5 kV peak-to-peak.

The total current profile during one half cycle of the applied potential shows again a few consecutive peaks, as is the case at lower applied potential (cf. Fig. 3 above for the "contact point model", but the same result was also obtained with the present model), but at this higher applied potential, the peaks are much stronger (up to 200 mA, vs 10-15 mA at lower applied potential), and they are not spaced apart evenly (see Fig. 11). The course of events shows a lot of similarities with the "contact point model" at higher applied potential. The periodic current peaks are caused by the sequence of different discharges as shown in Fig. 12. The reason why they happen in this order is explained by the electric field strength. As the applied voltage increases, the electric field strength in the reactor is also enhanced. The local discharges take place separately and consecutively, in an order depending on the time at which the necessary electric field strength is reached to create a breakdown in the gas. At the first three peaks, consecutive local glow-like discharges are formed in different regions: first in the gap between the two beads on the left (peak 1), then between the upper left bead and the dielectric layer (peak 2), and finally a simultaneous discharge between the dielectric layer and the top of the right bead and between the bottom of the right bead and the grounded electrode (peak 3). Afterwards, a discharge is formed over the whole gap distance, with plasma travelling through the so-called "channel of voids" from one wall to the other, corresponding to the most intense peak 4. This behaviour can be observed from Fig. 12, from top left to bottom right. Again, for the second half cycle similar discharges take place, but the timing relative to each other can change. Nevertheless, the strongest current peak always represents the discharge over the whole gap distance.

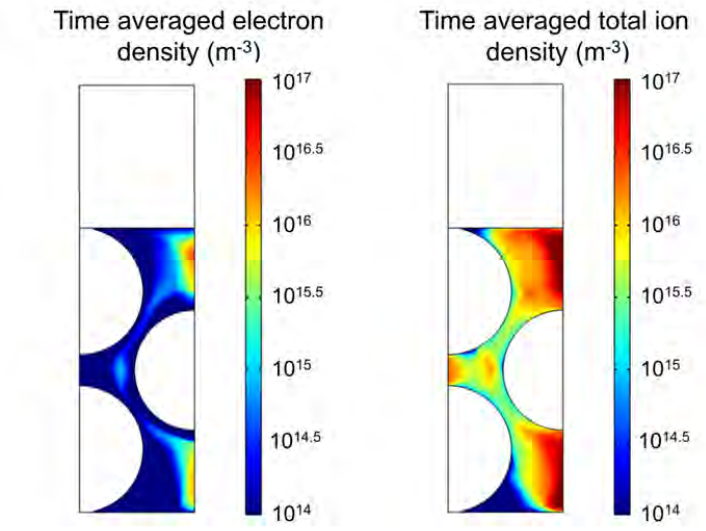

Fig. 13. Time averaged electron density (m^{-3}) and total ion density (m^{-3}) for an applied potential of 7.5 kV peak-to-peak.

Above and below the packing bead on the right, the time averaged electron density and total ion density reach a similar maximum value, around 10^{17} m^{-3}, which we call quasineutral (Fig. 13). However, closer to the walls, the electron density decreases much more than the ion density, corresponding to the sheath formation. Indeed, an average electron temperature of 3 eV and electron density of 10^{16} m^{-3} lead to a Debye length of 0.13 mm (~1/15 of the total width of the geometry). The narrow gaps in a packed bed geometry therefore will clearly show this sheath formation.

The stronger current peaks, the more or less quasineutral plasma in the bulk and the resulting lower electric field strength in these regions all indicate that the discharge behaves more or less like a glow discharge. The fact that the plasma can travel through the so-called "channel of voids" shows that it is of key importance to include this phenomenon when studying packed bed DBD reactors. However, it is important to note that when the "channel of voids" would not be present, and in other words the dielectric beads would be overlapping, discharges would still occur in the resulting individual pores. According to Pechereau et al., these discharges are even able to continue through the dielectric material, hopping from one pore to the other [36]. Nevertheless, we believe that when we want to investigate a real 3D packed bed DBD reactor by means of a 2D model, the presence of a "channel of voids" cannot be neglected.

Validation of our computational results with experimental data is not straightforward, because of the difficulty of plasma diagnostics due to the presence of a packing, as mentioned in the introduction. However, we can qualitatively compare our findings with experimental results reported by Kim et al. [37, 38], using an intensified charge coupled device (ICCD) camera. The authors studied a parallel plate DBD reactor in air, filled with two different types of packing material, namely $BaTiO_3$ (ε_r = 10000) and a silver-doped high-silica Y zeolite (Ag/HSY zeolite, ε_r = 4-5) with air as the discharge gas. The latter packing material is the most interesting for us, because its dielectric constant is closer to the value considered in our work (i.e., corresponding to zirconia). The authors observed that at lower input potential the discharge stays local at the contact points, but at higher potential, it also appears further away across the surface of the zeolite, in a form which they call "surface streamers". Tu et al. found some similar results using

a $BaTiO_3$ packing in a parallel plate DBD reactor with argon as the discharge gas [39]. When the input power was increased, the discharge evolved from a local filamentary discharge between nearby bead surfaces to a more extensive surface discharge. Finally, also Ye et al. saw the presence of a so-called surface discharge on the air- and sand-millets in a parallel plate DBD reactor, while in an empty reactor only filamentary discharges occurred [40]. These experimental results strongly resemble our computational results. Especially the work by Kim et al. and Tu et al. matches exactly our findings on the influence of the applied potential on the plasma formation in a PBPR, namely that at lower applied potential, a local discharge takes place, while at higher applied potential, the discharge has the ability to travel further away or to be formed elsewhere.

Regarding the values of electron density and ion density, we can only compare with other models, such as the helium model of Golubovskii et al. [31] and Massines et al. [33], since no experimental data is available. According to these papers, the density of the ions is typically up to two orders of magnitude higher than the electron density in a Townsend discharge, which is matched by our model (10^{15} versus 10^{13} m^{-3}). Furthermore, Golubovskii et al. found that the typical electron density at a current peak in a Townsend discharge is two orders of magnitude lower than for a glow discharge, which is also the case in our model (10^{17} versus 10^{19} m^{-3}). Finally, this model also learns us that the total current for a Townsend discharge is 1 to 2 orders of magnitude lower than the total current in a glow discharge. This all strengthens the idea that we are, indeed, dealing with Townsend and glow-like discharges, respectively.

Conclusion

We studied the behaviour of a PBPR by means of a fluid model. We applied two types of axisymmetric 2D models, i.e., a “contact point model” and a “channel of voids model”, to mimic as closely as possible the real 3D packed bed geometry, while avoiding excessively long calculation times. The results from the “contact point model” teach us that the plasma in a PBPR is initiated at the contact points, since this is the place with the highest electric field strength and thus the highest electron energy. When a low potential is applied, the plasma stays in this region, and shows the properties of a Townsend discharge. A higher applied potential will cause the discharge to further spread out into the bulk of the reactor towards the walls. The properties change to those of a glow discharge. The “channel of voids model” shows similar results. In this model, local Townsend discharges are also initiated at the position with high electric field strength, and they stay again in these regions at lower applied potential. When a higher potential is applied, glow-like discharges are formed, that can travel away from the contact points through the gaps between the contact points from one void to the other, ultimately covering the whole gas gap. It is therefore of uttermost importance to include this so-called “channel of voids” in a packed bed model, since the plasma will not stay localized when a higher potential is applied. These model results help us to obtain more insight in the plasma behaviour in a PBPR, which is difficult to obtain by plasma diagnostics.

Acknowledgements

The authors gratefully thank St. Kolev for the many interesting discussions and the useful advise in setting up the models. This research was carried out in the framework of the network on Physical Chemistry of Plasma-Surface Interactions - Interuniversity Attraction Poles, phase VII (http://psi-iap7.ulb.ac.be/), and supported by the Belgian Science Policy Office (BELSPO).

K. Van Laer is indebted to the Institute for the Promotion of Innovation by Science and Technology in Flanders (IWT Flanders) for financial support.

References

[1] A. Bogaerts, E. Neyts, R. Gijbels and J. van der Mullen, Spectrochimica Acta Part B, 57, 609-658 (2002)
[2] R. Aerts, W. Somers and A. Bogaerts, ChemSusChem, 8, 702-716 (2015)
[3] R. Snoeckx, Y.X. Zeng, X. Tu and A. Bogaerts, RSC Advances, 5, 29799-29808 (2015)
[4] S. Paulussen, B. Verheyde, X. Tu, C. De Bie, T. Martens, D. Petrovic, A. Bogaerts and B. Sels, Plasma Sources Sci. Technol., 19, 034015 (2010)
[5] H.L. Chen, H.M. Lee, S.H. Chen and M.B. Chang, Ind. Eng. Chem. Res. 47, 2122 (2008)
[6] K. Schmidt-Szalowski and A. Borucka, Plasma Chem. Plasma Proc., 9, 235 (1989)
[7] S. Jodzis, Ozone-Sci. Eng., 25, 63 (2003)
[8] H. L. Chen, H. M. Lee and M. B. Chang, Ozone: Sci. Eng., 28, 111 (2006)
[9] C.L. Chang and T.S. Lin, Plasma Chem. Plasma Proc., 25, 227 (2005)
[10] H.X. Ding, A.M. Zhu, X.F. Yang, C.H. Li and Y. Xu, J. Phys. D: Appl. Phys., 38, 4160 (2005)
[11] M. Kraus, B. Eliasson, U. Kogelschatz and A. Wonkaun, Phys. Chem. Chem. Phys., 3, 294 (2001)
[12] H.L. Chen, H.M. Lee, S.H. Chen, Y. Chao and M.B. Chang, Appl. Catal. B: Environ., 85, 1 (2008)
[13] Q. Yu, M. Kong, T. Liu, J. Fei and X. Zheng, Plasma Chem. Plasma Process., 32, 153-163 (2012)
[14] D. Mei, X. Zhu, Y. He, J.D. Yan and X. Tu, Plasma Sources Sci. Technol., 24, 015011 (2015)
[15] K. Van Laer and A. Bogaerts, Energy Technology, under publication
[16] A. Ohsawa, R. Morrow and A. Murphy, J. Phys. D: Appl. Phys., 33, 1487 (2000)
[17] J.S. Chang, K.G. Kostov, K. Urashima, T. Yamamoto, Y. Okayasu, T. Kato, T. Iwaizumi and K. Yoshimura, IEEE Trans. Ind. Appl., 36, 1251 (2000)
[18] K. Takaki, J.S. Chang and K.G. Kostov, IEEE Trans. Dielectr. Electr. Insul., 11, 481 (2004)
[19] W.S. Kang, J.M. Park, Y. Kim and S.H. Hong, IEEE Trans. Plasma Sci., 31, 504 (2003)
[20] H. Russ, M. Neiger and J.E. Lang, IEEE Trans. Plasma Sci., 27, 38 (1999)
[21] W.L. Morgan, Kinema Research & Software, LXcat database
[22] G.J.M. Hagelaar and L.C. Pitchford, Plasma Sources Sci. Technol., 14, 722 (2005)
[23] T. Martens, A. Bogaerts, W.J.M. Brok and J. van Dijk, Anal. Bioanal. Chem., 388, 1583-1594 (2007)
[24] Q. Wang, D.J. Economou and V.M. Donnelly, J. Appl. Phys., 100, 023301 (2006)
[25] P.L. Patterson, Phys. Rev. A, 2, 1154 (1970)
[26] B.E. Poling, J.M. Prausnitz, J.P. O'Connell, *The Properties of Gases and Liquids: Fifth Edition*, McGraw-Hill, New York, 11.5 (2001)
[27] M.M. Hafez, K. Oshima and D. Kwak, *Computational Fluid Dynamics Review 2010*, World Scientific Publishing, Singapore, 361 (2010)
[28] D. Petrovic, T. Martens, J. van Dijk, W.J.M. Brok and A. Bogaerts, *J. Phys.: Conf. Ser.*, 133, 012023 (2008)
[29] http://www.pardiso-project.org
[30] http://www.comsol.com

[31] Y.B. Golubovskii, V.A. Maiorov, J. Behnke and J.F. Benhke, J. Phys. D: Appl. Phys., 36, 39 (2003)
[32] V. Mikhailenko, J. Korean Vac. Soc., 21, 130-135 (2012)
[33] F. Massines, N. Gherardi, N. Naudé and P. Ségur, Plasma Phys. Control. Fusion, 47, B577 (2005)
[34] M. Bogaczyk, R. Wild, L. Stollenwerk and H.-E. Wagner, J. Phys. D: Appl. Phys., 45, 465202 (2012)
[35] A. Fridman, *Plasma Chemistry*, Cambridge University Press, Cambridge, 165 (2008)
[36] F. Pechereau, J. Jánsky and A. Bourdon, Plasma Sources Sci. Technol., 21, 055011 (2012)
[37] H.H. Kim, A. Ogata and Y.-H. Song, IEEE Trans. Plasma Sci., 39, 2220 (2011)
[38] H.H. Kim and A. Ogata, Int. J. Plasma Environ. Sci. Technol., 6, 43 (2012)
[39] X. Tu, H.J. Gallon and J.C. Whitehead, IEEE Trans. Plasma Sci., 39, 2172 (2011)
[40] Q. Ye, T. Zhang, F. Lu, J. Li, Z. He and F. Lin, J. Phys. D: Appl. Phys., 41, 025207 (2008)